ISSN 1070-3284, Russian Journal of Coordination Chemistry, 2018, Vol. 44, No. 1, pp. 64–71. © Pleiades Publishing, Ltd., 2018.

Syntheses, Crystal Structures, and Properties of Two IB Group Metal Coordination Polymers Based on 2-(Trifluoromethyl)-1H-Imidazole-4,5-Dicarboxylate[1]

S. L. Cai[a, *], H. M. Lin[a], J. R. Yang[a], Z. Q. He[a], S. Q. Fu[a], Z. B. Xu[a], S. R. Zheng[a, **], and W. G. Zhang[a, b]

[a]*School of Chemistry and Environment, South China Normal University, Guangzhou, 510006 P.R. China*

[b]*Guangdong YanJie Pharmatech Co. Ltd., Guangzhou, 510663 P.R. China*

**e-mail: songliangcai@m.scnu.edu.cn*

***e-mail: zhengsr@scnu.edu.cn*

Received April 24, 2017

Abstract—Two new IB group metal coordination polymers, namely, $\{[Cu_3(TFMIDC)_2(H_2O)_2] \cdot 4H_2O\}_n$ (**I**) and $[Ag_2(HTFMIDC)(Py)]_n$ (**II**) ($H_3TFMIDC$ = 2-(trifluoromethyl)-1H-imidazole-4,5-dicarboxylic acid, Py = pyridine), have been successfully prepared and structurally characterized by different techniques including single crystal X-ray diffraction (CIF files CCDC nos. 1545402 (**I**) and 1545403 (**II**)), IR spectra, and powder X-ray diffraction. Compound **I** features an interesting two-dimentional (2D) sheet containing 1D left-handed and right-handed helical chains, while compound **II** exhibits an infinite 1D zig–zag chain structure. Both two coordination polymers further stack through weak interactions to give rise to 3D supramolecular frameworks. Furthermore, the thermal stabilities of **I** and **II** as well as the photoluminescent property of **II** were also studied.

Keywords: imidazole-4,5-dicarboxylate, coordination polymer, hydrothermal synthesis, crystal structure

DOI: 10.1134/S1070328418010025

INTRODUCTION

In recent years, the coordination chemistry of 1H-imidazole-4,5-dicarboxylic acid (H_3IDC) [1–10] and its derivatives with various substituents at 2-position of the imidazole ring [11–35] has attracted considerable attention. This is because such a sort of N-heterocyclic carboxylic acid ligand can exhibit versatile coordination fashions under suitable hydro(solvo)thermal conditions. Indeed, by employing H_3IDC/functionalized H_3IDC and a variety of metal ions as building blocks, people have built up a great deal of desired 1D, 2D, and 3D metal-organic coordination polymers with intriguing structures, and found some of them may exhibit potential applications in the fields of gas absorption and separation [1–4], cation exchange [5–7], catalytic conversion [8, 9], chemical sensor [10–12], to name a few.

More recently, our group have introduced a trifluoromethyl group on the 2-position of H_3IDC and a new analogue ligand of H_3IDC, which is 2-(trifluoromethyl)-1H-imidazole-4,5-dicarboxylic acid ($H_3TFMIDC$), has been accordingly obtained [20]. We select $H_3TFMIDC$ as a potential bridging ligand to fabricate new coordination polymers on the basis of the following considerations: (i) Similar to the parent H_3IDC, the ligand $H_3TFMIDC$ that includes two imidazole N atoms and four carboxylate O atoms may display diverse coordination modes under appropriate reaction conditions. (ii) The introduced trifluoromethyl group, which is a strong electron-withdrawing group as compared to the other substituents such as methyl, ethyl and propyl groups, probably can affect the coordination ability/feature of the resulting $H_3TFMIDC$ ligand. (iii) The introduced trifluoromethyl group in the $H_3TFMIDC$ ligand also can be involved in hydrogen bonding interactions, such as C–H···F and O–H···F, thereby may lead to the formation of different supramolecular frameworks. In the previous studies, our group have successfully obtained a series of new coordination polymers from $H_3TFMIDC$ ligand, including 3D achiral/chiral main group metal coordination polymers bearing helical structures [19], 3D transition metal coordination polymers with diamondoid and (6,16)-connected topologies based on tetranuclear square building units [20], as well as 2D lanthanide coordination polymers with a honeycomb (6, 3) topology [21].

As a continuing exploration, in this paper, we will present the syntheses, crystal structures, and proper-

[1] The article is published in the original.

ties of two new IB group metal coordination polymers, $\{[Cu_3(TFMIDC)_2(H_2O)_2] \cdot 4H_2O\}_n$ (**I**) and $[Ag_2(HTFMIDC)(Py)]_n$ (**II**). To the best of our knowledge, no IB group metal coordination polymers derived from the $H_3TFMIDC$ ligand have been documented.

EXPERIMENTAL

Materials and measurements. The ligand $H_3TFMIDC$ was synthesized based on the previously reported procedure [20]. All the other chemicals were of analytical grade quality obtained from commercial vendors and used directly. Infrared (IR) spectra in the region of 400–4000 cm^{-1} was recorded on a Nicolet 5DX spectrometer using KBr pellet. Powder X-ray diffraction (PXRD) measurements were collected in the 2θ range of 5°–50° on a Bruker D8 Advance diffractometer at 40 kV, 40 mA with a Cu-target tube and a graphite monochromator. Thermogravimetric (TG) analyses were determined by utilizing a Perkin-Elmer TGA7 thermogravimetric analyzer with a heating rate of 10°C/min in flowing air atmosphere. The luminescent spectra for the solid state were performed on a Hitachi-2500 spectrophotometer with a 150 W xenon lamp as the light source at room temperature.

Synthesis of compound I. A mixture of $CuSO_4 \cdot 5H_2O$ (75 mg, 0.30 mmol), $H_3TFMIDC$ (67 mg, 0.30 mmol), Et_3N (0.15 mL), H_2O (2.0 mL) and EtOH (2.0 mL) was sealed in a 15 mL Teflon-lined stainless-steel autoclave, heated at 120°C for 48 h, and then cooled to room temperature at a rate of 5°C/h. Green block-shaped crystals of **I** were collected, washed with mother liquor, and dried in air in a yield of 57% (based on $H_3TFMIDC$).

IR (KBr; ν, cm^{-1}): 3650 w, 3490 s, 3343 w, 1644 w, 1563 s, 1496 w, 1461 s, 1387 s, 1275 m, 1205 w, 1184 m, 1155 w, 1131 m, 1039 w, 889 w, 842 w, 817 w, 792 w, 743 w, 593 w.

Synthesis of compound II. A mixture of $AgNO_3$ (102 mg, 0.60 mmol), $H_3TFMIDC$ (90 mg, 0.40 mmol), pyridine (0.25 mL), and EtOH (6.0 mL) was sealed in a 15 mL Teflon-lined stainless-steel autoclave and then heated at 140°C for 48 h under autogenous pressure. After cooling to room temperature at a rate of 5°C/h, brown rod-like crystals of **II** were obtained in a yield of 63% (based on $H_3TFMIDC$).

IR (KBr; ν, cm^{-1}): 3433 s, 2989 w, 1693 m, 1519 s, 1467 w, 1418 w, 1369 w, 1267 m, 1195 w, 1160 w, 1119 m, 1025 w, 990 w, 860 w, 789 w, 753 w, 704 w, 563 w.

X-ray crystallography. Single-crystal X-ray diffraction data collection for the compounds **I** and **II** were collected on a Bruker APEX II diffractometer employing graphite-monochromated MoK_α radiation (λ = 0.71073 Å) at 298 K. Both two structures were solved by direct methods using the SHELXS-2014 [36], and all the non-hydrogen atoms were refined anisotropically on F^2 by full-matrix least-squares technique utilizing the SHELXL-2014 program [37]. The hydrogen atoms on the water molecules were located from difference Fourier maps, while the other hydrogen atoms were placed in calculated positions and refined using a riding mode. Further details of the crystal parameters, data collections, and structural refinements for the compounds **I** and **II** are given in Table 1, whereas selected bond distances and angles with their estimated standard deviations are listed in Table 2.

Crystallographic data for **I** and **II** have been deposited with the Cambridge Crystallographic Data Centre (CCDC nos. 1545402 (**I**) and 1545403 (**II**); www.ccdc.cam.ac.uk/data_request/cif).

RESULTS AND DISCUSSION

The single crystal X-ray diffraction study reveals that the compound **I** displays an interesting 2D network bearing two different kinds of 1D helical chains. Its asymmetric unit comprises two crystallographically independent Cu^{2+} ions with site occupancies of 1 and 1/2, respectively, one completely deprotonated $TFMIDC^{3-}$ anion, one coordinated water molecule and two guest water molecules. The coordination environments of the Cu atoms are presented in Fig. 1a. The Cu(1) atom which locates on an inversion center is surrounded by two imidazole nitrogen atoms (N(2), $N(2)^i$) and two carboxylate oxygen atoms (O(4), $O(4)^i$) from two different $TFMIDC^{3-}$ ligands, with Cu–N and Cu–O bond lengths being 2.002(4) and 1.957(3) Å, respectively. Both the Cu(1)···O(2*w*) and Cu(1)···$O(2w)^i$ distances are equal to 2.498(4) Å, indicating weak interactions between the Cu and O atoms [38]. If these two long Cu(1)···O(2*w*) and Cu(1)···$O(2w)^i$ interactions are considered as bonds, the coordination geometry of Cu(1) atom can be described as elongated octahedral. The Cu(2) atom, however, is five-coordinated by one imidazole nitrogen atom (Cu–N 1.984(4) Å) and three carboxylate oxygen atoms (Cu–O 1.933(3)–2.080(4) Å) from two distinct $TFMIDC^{3-}$ ligands and one oxygen atom (Cu–O 1.997(4) Å) from a coordinated water molecule to generate a distorted square pyramidal sphere. It is noteworthy to mention that two carboxyl groups and one imidazole N–H group of the $H_3TFMIDC$ ligand in compound **I** are all deprotonated, and the resulting $TFMIDC^{3-}$ anion adopts an unique coordination mode, namely μ_3-*k*N,O: *k*N',O': *k*O'',O''' to simultaneously connect one Cu(1) and two Cu(2) ions in bis-N,O-chelating and O,O'-chelating fashions, as illustrated in Scheme 1a:

Table 1. Crystallographic data and structure refinements for the compounds **I** and **II**

Parameter	Value	
	I	**II**
Empirical formula	$C_{12}H_{12}N_4O_{14}F_6Cu_3$	$C_{11}H_6N_3O_4F_3Ag_2$
Formula weight	740.88	516.93
Temperature, K	298(2)	298(2)
Crystal system	Monoclinic	Monoclinic
Space group	$P2_1/n$	$P2_1/c$
a, Å	6.4551(9)	11.0790(11)
b, Å	8.7249(13)	17.0967(17)
c, Å	19.436(3)	7.1403(8)
β, deg	91.218(2)	91.926(10)
V, Å^3	1094.4(3)	1351.7(3)
Z	2	4
ρ_{calcd}, mg m^{-3}	2.248	2.540
μ, mm^{-1}	3.021	2.957
F(000)	730	984
θ Range for data collection, deg	2.096–25.246	3.010–25.244
Max, min transmission	0.636, 0.526	0.756, 0.525
Reflections collected	5459	5138
Unique reflections	1977	2434
Reflections with $I > 2\sigma(I)$	1481	1909
R_{int}	0.0818	0.0786
R_1*, wR_2** ($I > 2\sigma(I)$)	0.0444/0.1121	0.0553/0.1357
R_1*, wR_2** (all data)	0.0655/0.1269	0.0711/0.1479
Goodness-of-fit on F^2	1.063	1.040
$\Delta\rho_{max}$ and $\Delta\rho_{min}$, e Å^{-3}	0.570/–0.515	1.773/–1.287

* $R_1 = \Sigma\|F_o| - |F_c\|/\Sigma|F_o|$, ** $wR_2 = \{\Sigma[w(F_o^2 - F_c^2)^2]/\Sigma(F_o^2)^2\}^{1/2}$.

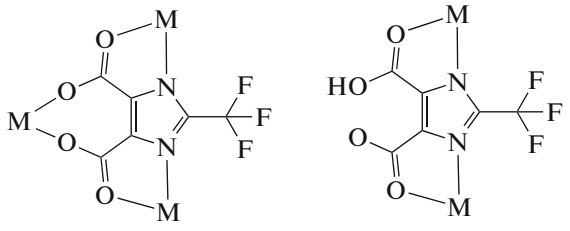

Scheme 1.

In the crystal structure of compound **I**, the neighbouring Cu(2) atoms are alternately bridged by the TFMIDC^{3-} ligands employing the N,O-chelating and O,O'-chelating coordination sites to give rise to the formation of interesting 1D left-handed and right-handed helical chains running along the crystallographic 2_1 screw axis, as depicted in Fig. 2a. The pitches of the two helical chains are the same and equal to the unit cell length of the y axis (8.7249(13) Å), while the adjacent nonbonding Cu(2)···Cu(2) distances in two types of helical chains are all equal to 5.7459(10) Å. These 1D left-handed and right-handed helical chains are then linked each other via the shared Cu(1) centers, leading to the construction of an achiral 2D layer in the yz plane, as described in Fig. 2b. From a topological viewpoint, such a 2D layer structure can be simplified as a (6, 3) topological network if the TFMIDC^{3-} units are considered as 3-connected nodes, and both Cu(1) and Cu(2) ions are viewed as spacers. Additionally, the 2D sheets are stacked along the x direction in an –AAA– sequence through diverse O–H···O and O–H···F hydrogen bonding interactions involving the coordinated and uncoordinated water molecules as well as the carboxyl group and trifluoromethyl group of the TFMIDC^{3-} ligand, thereby producing a 3D microporous supramolecular framework (Figs. 2c, 2d). The

Table 2. Selected bond lengths (Å) and angles (deg) for the compounds **I** and **II**

Bond	*d*, Å	Bond	*d*, Å	Bond	*d*, Å
		I			
Cu(1)–N(2)	2.002(4)	Cu(2)–N(1)	1.984(4)	Cu(2)–O(2)$^{\#2}$	2.044(4)
Cu(1)–O(4)	1.957(3)	Cu(2)–O(3)$^{\#2}$	1.933(3)	Cu(2)–O(1)	2.080(4)
Cu(1)–O(2*w*)	2.498(4)	Cu(2)–O(1*w*)	1.997(4)		
		II			
Ag(1)–N(3)	2.149(6)	Ag(1)–N(1)	2.155(6)	Ag(2)–N(2)	2.148(7)
Ag(2)–O(1)$^{\#1}$	2.170(6)				
Angle	ω, deg	Angle	ω, deg	Angles	ω, deg
		I			
O(4)Cu(1)N(2)	82.85(15)	N(1)Cu(2)O(1*w*)	98.67(17)	O(3)$^{\#2}$Cu(2)O(1)	87.27(14)
O(4)Cu(1)O(2*w*)	88.19(16)	O(3)$^{\#2}$Cu(2)O(2)$^{\#2}$	96.23(15)	N(1)Cu(2)O(1)	80.85(15)
N(2)Cu(1)(2*w*)	89.61(15)	N(1)Cu(2)O(2)$^{\#2}$	90.91(15)	O(1*w*)Cu(2)O(1)	123.8(2)
O(3)$^{\#2}$Cu(2)N(1)	167.93(16)	O(1*w*)Cu(2)O(2)$^{\#2}$	120.36(19)	O(2)$^{\#2}$Cu(2)O(1)	115.86(16)
O(3)$^{\#2}$Cu(2)O(1*w*)	86.12(16)				
		II			
N(3)Ag(1)N(1)	173.0(2)	N(2)Ag(2)O(1)$^{\#1}$	172.3(2)		

* Symmetry transformations used to generate equivalent atoms: $^{\#1}$ $-x, -y, -z$; $^{\#2}$ $-x-1/2, y+1/2, -z+1/2$ (**I**); $^{\#1}$ $-x+2, y-1/2, -z+1/2$ (**II**).

samll pores are opened along the *x*-axial direction (Fig. 2d), and are filled with guest water molecules. PLATON [39] analysis indicates that compound **I** contains a small potential solvent volume of 136.6 Å^3 (12.5%) if only the free water molecules of O(2*w*) and O(3*w*) are removed.

Single crystal structure determination indicates that compound **II** exhibits an infinite 1D zig–zag chain structure. The relevant asymmetric unit of this compound consists of two crystallographically independent Ag(I) cations, one HTFMIDC^{2-} anion and one coordinated pyridine neutral molecule. As shown in Fig. 1b, each Ag(1) atom is completed by two nitrogen atoms (N(1), N(2)), of which one is from a HTFMIDC^{2-} ligand, and the other is from a pyridine ligand. While each Ag(2) atom is defined by one imidazole nitrogen atom (N(2)) and one carboxylate oxygen atom (O(1)^{i}) from two different HTFMIDC^{2-} ligands. The Ag–O bond length is 2.170(6) Å, and the Ag–N distances vary from 2.148(7) to 2.155(6) Å, whereas the bond angles around Ag(1) and Ag(2) ions are 173.0(2)° and 172.3(2)°, respectively, all of which fall in the normal range. It is important to note that the distances of Ag(1)···O(1) and Ag(2)···O(4) are equal to 2.651(5) and 2.656(6) Å, respectively, which are significantly shorter than sum of the corresponding van der Waals radii (3.1 Å), again implying weak interactions between these Ag and O atoms [40]. Thus, both Ag(1) and Ag(2) atoms are three-coordinated with a distorted T-shaped coordination geometry if the both the weak Ag(1)···O(1) and Ag(2)···O(4) interactions are seen as bonds. And in this case, the doubly deprotonated HTFMIDC^{2-} ligand employs a coordination fashion called μ_2-*k*N,O: *k*N',O' to connect one Ag(1) and one Ag(2) ions in bis-N,O-chelating mode, as displayed in Scheme 1b. An intramolecular hydrogen bond can be found between the uncoordinated carboxylic acid/carboxylate atoms of the HTFMIDC^{2-} ligand (O(3)–H(3)···O(2), H···O 1.68, O···O 2.500(8) Å, ∠OHO 173°).

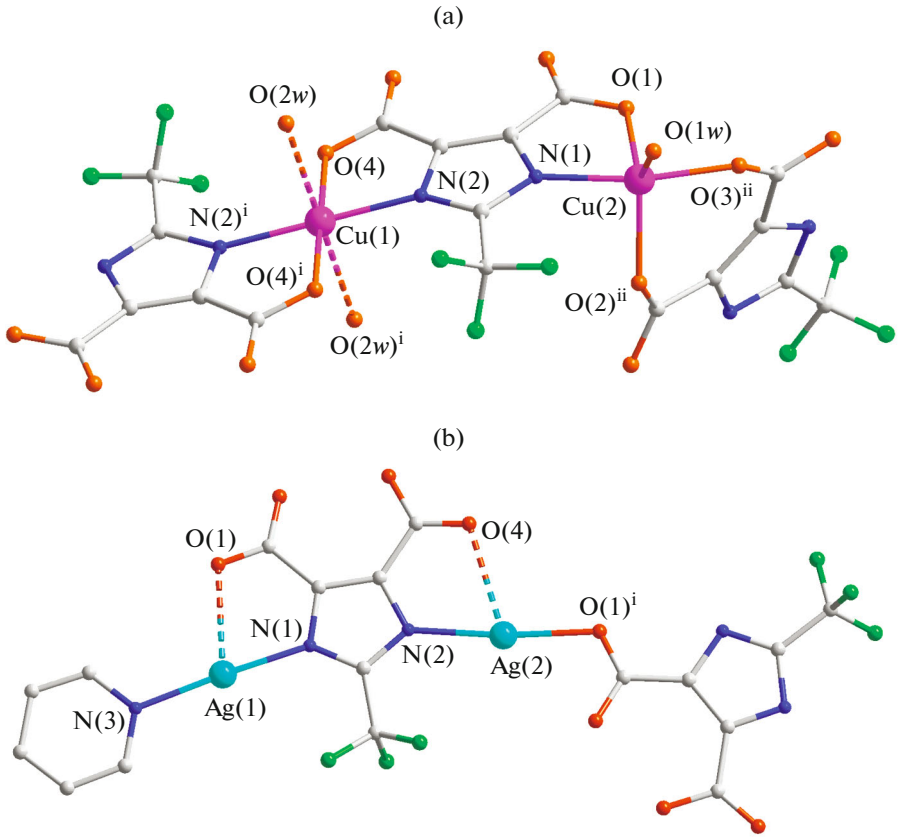

Fig. 1. The coordination environment of Cu^{2+} ions in **I** (a) and Ag(I) ions in **II** (b). The hydrogen atoms are omitted for clarity. Symmetry codes: (i) $-x, -y, -z$; (ii) $-x - 1/2, y + 1/2, -z + 1/2$ (a); (i) $-x + 2, y - 1/2, -z + 1/2$ (b).

In compound **II**, the Ag(1) and Ag(2) ions are alternately connected by the $HTFMIDC^{2-}$ units based on the above-mentioned coordination fashion, resulting in the formation of an infinite 1D zig–zag chain running parallel to the crystallographic *y* axis (Fig. 3a), in which the adjacent nonbonding Ag···Ag separations are 4.498(2) and 6.412(2) Å, respectively. Various weak hydrogen bonds including C–H···F and C–H···O formed between pyridine ligand and the trifluoromethyl or carboxyl groups of the $TFMIDC^{3-}$ ligand further assemble these 1D zig–zag chains into a 2D supramolecular network, as illustrated in Fig. 3a. Moreover, the 2D layers are packed along the *z*-axial direction in an –ABAB– fashion through π···π stacking interactions formed between neighbouring imidazole rings (centroid–centroid distance, 3.396 Å) and between adjacent pyridyl rings (centroid–centroid distance, 3.929 Å) to give rise to a 3D supramolecular framework as shown in Fig. 3b.

The IR spectra of compounds **I** and **II** were measured by employing KBr pellets in 400–4000 cm^{-1} range. Both two compounds display strong and broad peaks at around 3450 cm^{-1}, which can be attributed to the characteristic peaks of O–H vibrations from the coordinated and free water molecules. The absence of the intense absorption peak around 1700 cm^{-1} in the IR spectrum of compound **I** suggests that two carboxylate groups of $H_3TFMIDC$ ligand have been completely deprotonated. While for compound **II**, a medium strong absorption peak centered at 1693 cm^{-1} is observed in its IR spectrum, indicating that the carboxylate groups of $H_3TFMIDC$ ligand are just partly deprotonated. Additionally, both two samples present strong bands at about 1630–1500 and 1430–1330 cm^{-1}, which may be attributable to the asymmetric stretches (ν_{as}) and symmetric stretches (ν_s) of the carboxylate groups, respectively [41]. Basically, the IR spectral data of compounds **I** and **II** are in well agreement with their corresponding X-ray single-crystal structures.

In order to ensure the phase purity of the as-synthesized bulky products, PXRD experiments for compounds **I** and **II** have been measured at room temperature and the results are presented in Fig. 4. As can be noted, most of the peaks appeared in the experimental patterns corroborate quite well with those produced from single crystal X-ray diffraction data, which apparently indicates the crystalline phase homogeneity of both two compounds. The dissimilarities in

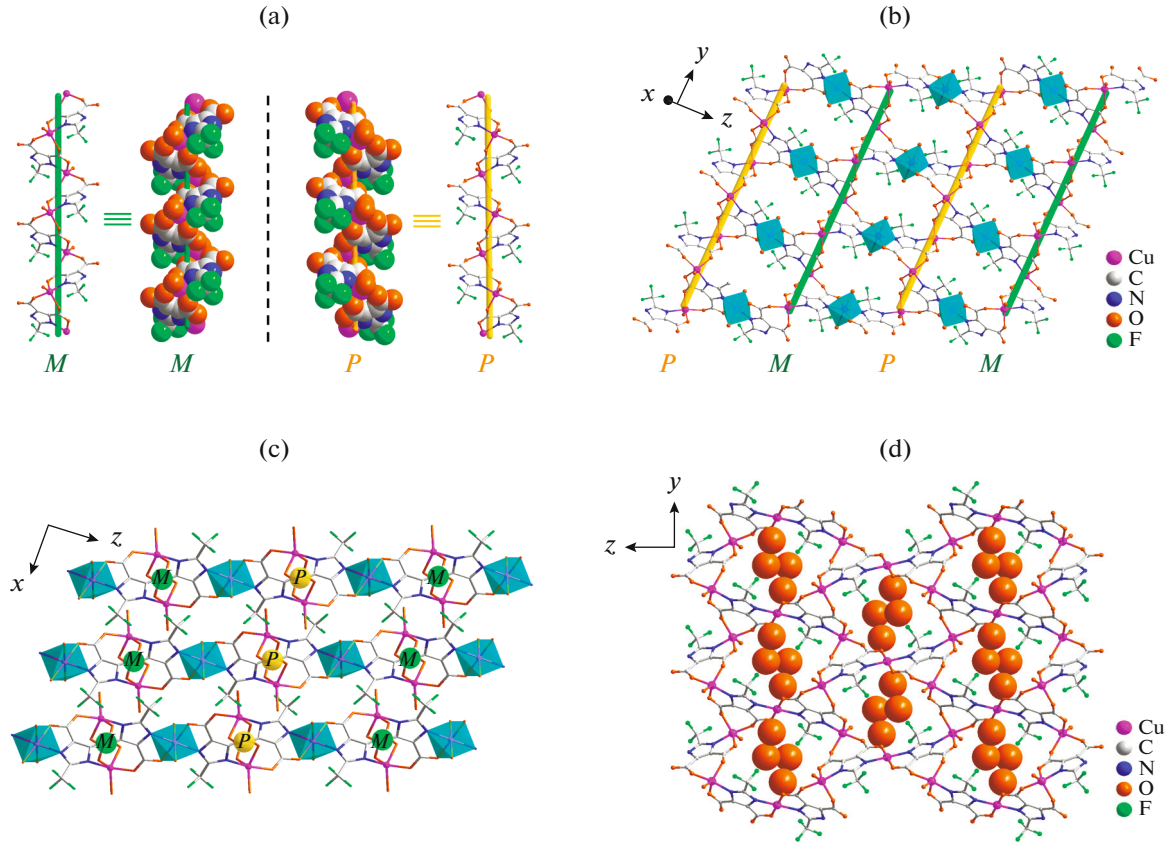

Fig. 2. Ball-and-stick and space-filling views of the 1D helical chains in compound **I** (a) (the chirality of each helical is labeled *M* (left-handed) or *P* (right-handed); view of the achiral 2D layer in compound **I**, which is built by the connection of the alternate left-handed and right-handed helical chains via the shared Cu(1) centers (b); the 3D supramolecular network of compound **I** viewed down along *y* axis (c); the 3D supramolecular network of compound **I** viewed down along *x* axis, showing small pores filled with guest water molecules (d).

reflection intensity between the simulated and the measured patterns are probably due to the preferred orientation of the powder samples during data collection.

To examine the thermal stabilities of the coordination polymers, TG analyses of **I** and **II** were carried out in the temperature of 30–800°C under air atmosphere with a heating rate of 10°C min^{-1}, and their TG curves are shown in Fig. 5. For compound **I**, the first weight loss of 9.4% from 46 to 93°C can be attributable to the release of two free water molecules (calcd. 9.7%) in the asymmetric unit, while the second weight loss of 4.6% from 93 to 148°C may be ascribed to the departure of one coordinated water molecule (calcd. 4.9%). Then the solvent-free network of compound **I** is stable up to approximately 335°C, and further weight loss above 335°C is assigned to the decomposition of the whole coordination framework. For compound **II**, no obvious weight loss can be observed before the temperature of about 250°C, which demonstrates that the supramolecular framework of **II** is stable up to 250°C. Further increasing the temperature leads to the collapse of the whole framework.

According to the previously reported literature, coordination polymers containing Ag(I) ions usually exhibit well photoluminescent properties. Hence, the solid-state emission spectra of compound **II** as well as the free H_3TMFIDC ligand were investigated at room temperature. As described in Fig. 6, the intense bands in the emission spectrum of compound II can be found at 502 and 533 nm upon excitation at 362 nm. Compared with the free ligand H_3TMFIDC (the emission at 447 nm with λ_{ex} = 368 nm), the largely red-shift emission for compound **II** can probably be attributed to ligand-to-metal charge transfer (LMCT) [42, 43].

ACKNOWLEDGMENTS

We gratefully acknowledge the financial support by the National Natural Science Foundation of P.R. China (grants nos. 21603076, 21571070 and

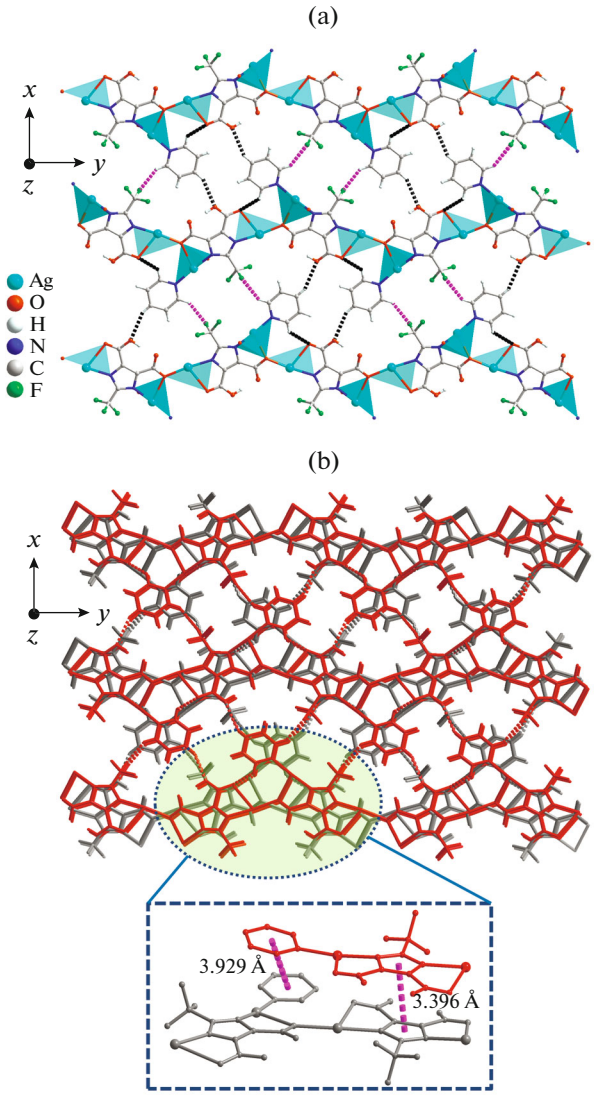

Fig. 3. View of the 2D supramolecular network in compound **II**, which is constructed from the connection of adjacent 1D zig–zag chains through various C−H···F and C−H···O weak hydrogen bonds (a); view of the 3D supramolecular framework in compound **II** assembled by two different types of π···π stacking interactions (b).

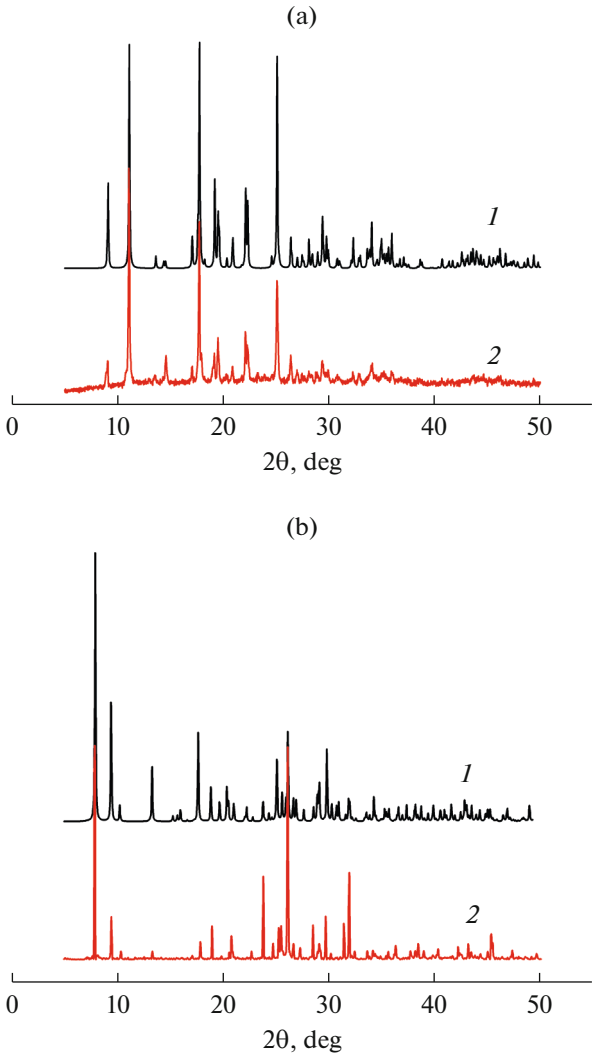

Fig. 4. The simulated PXRD patterns (*1*) and the experimental ones (*2*) for compound **I** (a) and compound **II** (b).

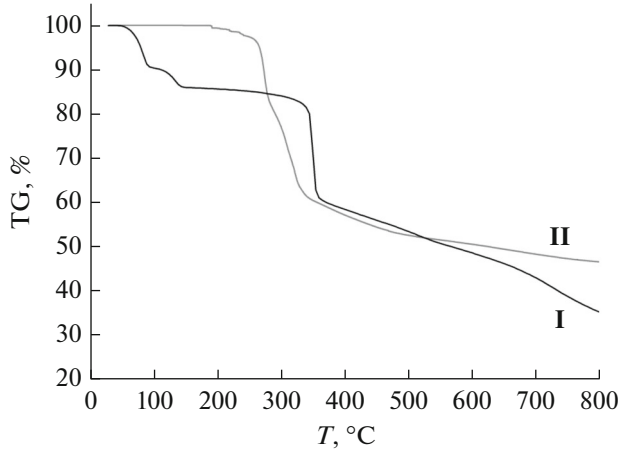

Fig. 5. The TGA curves for the compounds **I** and **II**.

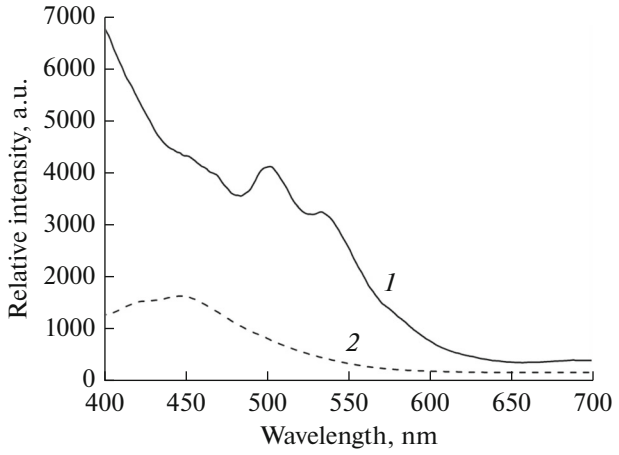

Fig. 6. The solid state emission spectra of compound **II** (*1*) and the free H_3TMFIDC ligand (*2*) at room temperature.

21473062), the Natural Science Foundation of Guangdong Province (grant no. 2016A030310437), the SCNU Foundation for Fostering Young Teachers (grant no. 15KJ02), and the Undergraduates' Innovating Experimentation Project of SCNU and Guangdong Province (grant no. hx201622).

REFERENCES

1. Maji, T.K., Mostafa, G., Chang, H.C., and Kitagawa, S., *Chem. Commun.*, 2005, p. 2436.
2. Zou, R.Q., Jiang, L., Senoh, H., et al., *Chem. Commun.*, 2005, p. 3526.
3. Gu, Z.G., Cai, Y.P., Fang, H.C., et al., *Chem. Commun.*, 2010, vol. 46, p. 5373.
4. Peralta, D., Chaplais, G., Simon-Masseron, A., et al., *J. Chem. Soc.*, 2012, vol. 134, p. 8815.
5. Lu, W.G., Jiang, L., Feng, X.L., and Lu, T.B., *Inorg. Chem.*, 2009, vol. 48, p. 6997.
6. Liu, Y., Kravtsov, V.C., Larsen, R., and Eddaoudi, M., *Chem. Commun.*, 2006, p. 1488.
7. Nouar, F., Eckert, J., Eubank, J.F., et al., *J. Am. Chem. Soc.*, 2009, vol. 131, p. 2864.
8. Zou, R.Q., Sakurai, H., and Xu, Q., *Angew. Chem. Int. Ed.*, 2006, vol. 45, p. 2542.
9. Alkordi, M.H., Liu, Y.L., Larsen, R.W., et al., *J. Am. Chem. Soc.*, 2008, vol. 130, p. 12639.
10. Ding, Y.J., Li, T., Hong, X.J., et al., *CrystEngComm*, 2015, vol. 17, p. 3945.
11. Shi, B.B., Zhong, Y.H., Guo, L.L., and Li, G., *Dalton Trans.*, 2015, vol. 44, p. 4362.
12. Cai, S.L., Zheng, S.R., Fan, J., et al., *Inorg. Chem. Commun.*, 2011, vol. 14, p. 937.
13. Cai, S.L., Zheng, S.R., Wen, Z.Z., et al., *Cryst. Growth Des.*, 2012, vol. 12, p. 2355.
14. Cai, S.L., Zheng, S.R., Wen, Z.Z., et al., *Cryst. Growth Des.*, 2012, vol. 12, p. 5737.
15. Cheng, M.L., Han, W., Liu, Q., et al., *J. Coord. Chem.*, 2014, vol. 67, p. 215.
16. Zhang, F.W., Li, Z.F., Ge, T.Z., et al., *Inorg. Chem.*, 2010, vol. 49, p. 3776.
17. Feng, X., Zhao, J.S., Liu, B., et al., *Cryst. Growth Des.*, 2010, vol. 10, p. 1399.
18. Feng, X., Miao, S.B., Li, T.F., and Wang, L.Y., *Russ. J. Coord. Chem.*, 2011, vol. 37, p. 572.
19. Li, T.T., Huang, X., Guo, J.G., et al., *Inorg. Chem. Commun.*, 2014, vol. 48, p. 61.
20. Cai, S.L., Zheng, S.R., Fan, J., et al., *CrystEngComm*, 2016, vol. 18, p. 1174.
21. Cai, S.L., Zhang, K., Wang, S., et al., *Struct. Chem.*, 2017, vol. 28, p. 577.
22. Zheng, S.R., Cai, S.L., Pan, M., et al., *CrystEngComm*, 2011, vol. 13, p. 883.
23. Cai, S.L., Zheng, S.R., Wen, Z.Z., et al., *Cryst. Growth Des.*, 2012, vol. 12, p. 3575.
24. Li, T.T., Cai, S.L., Zeng, R.H., et al., *Inorg. Chem. Commun.*, 2014, vol. 48, p. 40.
25. Li, X., Wu, B.L., Niu, C.Y., et al., *Cryst Growth Des.*, 2009, vol. 9, p. 3423.
26. Wang, W.Y., Niu, X.L., Gao, Y.C., et al., *Cryst Growth Des.*, 2010, vol. 10, p. 4050.
27. Sang, Y.L., Xin, J.F., and Gao, R.M., *Russ. J. Coord. Chem.*, 2016, vol. 42, p. 410.
28. Wang, C.J., Wang, T., Li, L., et al., *Dalton Trans.*, 2013, vol. 42, p. 1715.
29. Xie, L.X., Hou, X.W., Fan, Y.T., et al., *Cryst. Growth Des.*, 2012, vol. 12, p. 1282.
30. Zhang, Y., Guo, B.B., Li, L., et al., *Cryst. Growth Des.*, 2013, vol. 13, p. 367.
31. Gao, R.M., Li, J., Guo, M.W., and Li, G., *Russ. J. Coord. Chem.*, 2014, vol. 40, p. 379.
32. Wang, F., Chen, Z.N., Li, Z.F., and Li, G., *Russ. J. Coord. Chem.*, 2015, vol. 41, p. 510.
33. Yao, M.J., Ren, X., Yue, Z.F., and Li, G., *Russ. J. Coord. Chem.*, 2015, vol. 41, p. 524.
34. Lin, Y.J., Shan, W.L., and Jin, G.X., *Dalton Trans.*, 2014, vol. 45, p. 12680.
35. Cai, S.L., Wang, S., He, Z.H., et al., *Z. Anorg. Allg. Chem.*, 2017, vol. 643, p. 593.
36. Sheldrick, G.M., *Acta Crystallogr., Sect. A: Found. Adv.*, 2015, vol. 71, p. 3.
37. Sheldrick, G.M., *Acta Crystallogr., Sect C: Cryst. Chem.*, 2015, vol. 71, p. 3.
38. Yang, L., Powell, D.R., and Houser, R.P., *Dalton Trans.*, 2007, p. 955.
39. Spek, A.L., *PLATON, A Multipurpose Crystallographic Tool*, Utrecht: Utrecht University, 2005.
40. Zhao, B., Zhao, X.Q., Shi, W., and Cheng, P., *J. Mol. Struct.*, 2007, vol. 830, p. 143.
41. Yue, Z.F., Chen, Z.N., Zhong, Y.H., and Li, G., *J. Coord. Chem.*, 2015, vol. 68, p. 2507.
42. Tao, J., Shi, J.X., Tong, M.L., et al., *Inorg. Chem.*, 2001, vol. 40, p. 6328.
43. Zhang, Y.N., Wang, H., Liu, J.Q., et al., *Inorg. Chem. Commun.*, 2009, vol. 12, p. 611.